Evolution mechanism of Pinghu Formation coal-measure source rock from the Xihu Sag, East China Sea basin: Evidence from carbon isotopic evolution of kerogen, oil, and gas during hydrous pyrolysis

Qiang Cao[1], Jiaren Ye*, [1], Yongchao Lu[1], Yang Tian[2, *], Jinshui Liu[3], Chenjie Xu[1], Hanwen Yu[1], Lina Sun[2]

[1]Key Laboratory of Tectonics and Petroleum Resources, China University of Geosciences, Ministry of Education, Wuhan 430074, China;

[2]Hubei Cooperative Innovation Center of Unconventional Oil and Gas, Yangtze University, Wuhan, Hubei 430100, China;

[3] CNOOC Shanghai Branch Shanghai 200030, China.

*Corresponding author (First). Jiaren Ye; Tel. 86-27- 67883295; Email address: jrye@cug.edu.cn;

Corresponding author (Second). Yang Tian; Tel. 86-27- 69111832; Email address: 519974963@qq.com.

Abstract: Semi-open hydrous pyrolysis experiments on coal-measure source rocks in the Xihu Sag were conducted to investigate the carbon isotope evolution of kerogen, bitumen, generated expelled oil, and gases with increasing thermal maturity. Seven experiments corresponding were conducted at 335 °C, 360 °C, 400 °C, 455 °C, 480 °C, 525 °C, and 575 °C, while other experimental factors, such as the heating time and rate, lithostatic and hydrodynamic pressures, and columnar original samples were kept the same. The results showed that the simulated temperatures were positive for the measured vitrinite reflectance (*Ro*), with a correlation coefficient (R^2) of 0.9861. With increasing *Ro*, lower maturity, maturity, higher maturity, and post-maturity stages occurred at simulated temperatures (*Ts*) of 335–360 °C, 360–400 °C, 400–480 °C, and 480–575 °C, respectively. The increasing gas hydrocarbons with increasing *Ro* reflected the higher gas potential. Moreover, the carbon isotopes of kerogen, bitumen, expelled oil, and gases were associated with an increased *Ro*; among gases, methane was the most sensitive to *Ro*. Ignoring the intermediate reaction process, the thermal evolution process can be summarized as $kerogen_0$ *(original) + bitumen*$_0$ *(original)* $\rightarrow$ $kerogen_r$ *(residual kerogen) + expelled oil (generated) + bitumen*$_{n+r}$ *(generated + residual) +* C_{2+} *(generated + residual) +* CH_4 *(generated).* Among these, bitumen, expelled oil, and $C_{2\text{-}5}$ acted as reactants and products, whereas kerogen and methane were the reactants and products, respectively. Furthermore, the order of the carbon isotopes during the thermal evolution process was identified as: $^{13}C_{\ 1} < {}^{13}C_{\ 2\text{-}5} < {}^{13}C_{\ \text{expelled oil}} < {}^{13}C_{\ \text{bitumen}} < {}^{13}C_{\ \text{kerogen}}$. Thus, the reaction and production mechanisms of carbon isotopes can be obtained based on their changing degree and yields in kerogen, bitumen, expelled oil, and gases. Furthermore, combining the analysis of geochemical characteristics of the Pinghu Formation coal-oil-type gas in actual strata with these pyrolysis experiments, it was identified that this area also had substantial development potential. Therefore, this study provides theoretical

support and guidance for the formation mechanism and exploration of oil and gas in the Xihu Sag.

Keywords: coal-measure source rock; Xihu Sag; semi-open hydrous pyrolysis; carbon isotope; maturity; reaction mechanism

1. Introduction

The East China Sea Shelf Basin (ECSSB) is an important petroliferous basin in the eastern coastal areas of China, and the corresponding coal-measure strata of Neogene are thick and widely distributed. In recent years, the increasing intensity of research and development pertaining to oil and gas exploration, have revealed the crucial role played by the relevant coal-measure source rock in the formation of oil and gas resources in this area (Zhu et al., 2012; Ju et al., 2016; Chen et al., 2017; Hao et al., 2018; Zhu et al., 2019). The Xihu Sag is located northeast of the ECSS, and the source rocks are primarily developed in the Pinghu, Huagang, and Longjing formations (Su et al., 2018; Zhu et al., 2012). In particular, the coal rock of the Pinghu Formation is the primary source rock in the Xihu Sag and is characterized by its large thickness and wide distribution (Zhang et al., 2006; Lin et al., 2017; Xie et al., 2018; Cheng et al.,2019; Wang et al., 2021). Thus, determining the formation mechanism of thermal evolution is particularly important for understanding oil and gas evolution in this area.

However, previous studies on the thermal evolution of organic matter have concentrated primarily on basic geology (such as petroleum sources, evolution and origin of paleo-pressure, diagenetic and reservoir-forming processes, and geochemical characteristics) (Jiang et al., 2016; Hao et al., 2018; Cheng et al., 2020; Su et al., 2019; Wang et al., 2020; Xu et al., 2020). These studies primarily utilized geological and geochemical methods, and the research contents were often limited by static characteristics such as hydrocarbon generation potential and maturity of source rocks (Tissot et al., 1974). In addition, during the process of geological burial in source rocks, the generation of oil and gas, as well as their occurrence in the ground, were the comprehensive responses of various physical and chemical actions. Compared to the changeable and complex geological evolution process and the scale of human life, the evolution of organic matter was exceedingly slow, such that it was impossible to observe the thermal evolution process with variable temperature and pressure, such as hydrocarbon cracking in the system. Thus, it is extremely challenging to accurately describe the generation of oil and gas (Lewan et al., 1979; Lewan, 1997; Braun and Bumham, 1990; Schimmelmann et al. 2001 Hill et al., 2007). With the development and progress of science and technology and petroleum geology theory, scientists have gradually realized the importance of investigating hydrocarbon generation and expulsion of source rocks during the thermal evolution process (Connan, 1974; Pepper et al., 1995a and 1995 b). However, there are hurdles such as dissimilar understanding and lack of accord among researchers on hydrocarbon generation and expulsion simulations, potential calculation methods, and migration mechanisms; thus, it became necessary to simulate the organic evolution process in source rocks through a simulated pyrolysis experiment (Behar et al.,

1992; Leif et al., 2000; Sun et al., 2015; Sun et al., 2019a). The principle of the hydrocarbon generation and expulsion simulated experiments was to use short time and high-temperature conditions to simulate and observe the evolution of organic matter under long-term and low-temperature conditions in actual geological conditions (Castelli et al., 1990; Leif et al., 2000; Sun et al., 2019b). Thus, through simulation experiments of hydrocarbon generation and expulsion in the laboratory, we could obtain information, such as the amount of hydrocarbon generation in different evolution stages and the composition characteristics of gases at different maturity levels, that was otherwise difficult to obtain in the natural evolution process. However, there have been few studies on the pyrolysis experiments of coal-measure source rocks of the Pinghu Formation in the Xihu Sag. In the closed simulated system, based on the methods of fluid inclusion analysis, petroleum geochemistry, and rock gold-tube pyrolysis on the condensates in the Pinghu slope belt of the Xihu Sag, Su (2020) found that coal was evaluated as source rock and inclined to gas and oil generation at moderate maturity. In an open simulated system, Zhu (2020) used the Rock-Eval pyrolysis method to analyze the organic geochemical and petrographic characteristics of Paleogene coals and organic-rich mudstones in the Xihu Sag and found that two different regions had fair to excellent hydrocarbon generative potential but varied in the hydrocarbon phase. However, almost no pyrolysis experiments have been conducted on the coals of the Pinghu Formation under the semi-open system.

Moreover, based on the principle of chemical kinetics, different zero-point energies between carbon isotopes cause differences in chemical activity, which would result in the formation of structural parts or chemical bonds (^{12}C–^{12}C) rich in light carbon isotopes with a preference to participate in the reactions. During hydrocarbon generation, it was more difficult for branched chains with more ^{13}C to fall off than those with less ^{13}C. Thus, during the thermal evolution of organic matter into hydrocarbons, the first products to be generated were relatively enriched in ^{12}C, and subsequent products were relatively enriched in ^{13}C (Krouse et al., 1988; Waples, 2000; Zhao et al., 2015; Fu et al., 2020). The contributions of different genesis and origin source rocks to oil and gas generation may be influenced by the thermal evolution, depositional environment, and mixing of organic matter from multiple source rocks. Simultaneously, the differences in organic matter with specific sources could be corrupted or integrated by the measured compositions of bulk isotopes and molecules (Xu et al., 2020). Moreover, studying the characteristics of carbon isotopes can reveal information of parent material sources and also assess natural gas with different origins and thermal evolution degrees (Prinzhofer and Huc, 1995; Cramer et al., 1998; Dai et al., 2009; Takahashi et al., 2014; Wu et al., 2019; Xu et al., 2020). Thus, it is of great significance to comprehensively study the carbon isotopic composition of kerogen, bitumen, and gas-liquid products during thermal evolution.

This study focused on the pyrolysis of coal-measure source rocks in the Pinghu Formation under a semi-open system with varying simulated conditions (such as temperature, static pressure, fluid pressure, time, water addition, and origi-

nal columnar samples) to determine the main factors affecting the evolution of organic matter. The advantage of the semi-open system was that it considered several influencing factors and was closer to the actual geological conditions. It has also been known from a large number of pyrolysis experiments domestically and internationally that the hydrocarbon generation potential of source rocks can be determined by the content of organic matters in source rocks. In contrast, the hydrocarbon generation and expulsion characteristics of source rocks were affected by many factors, including temperature, pressure, hydrocarbon generation space and porosity, and presence of water and catalysts (Lewan et al., 1979; Behar et al., 1992; Schimmelmann et al., 2001; Sun et al., 2015; Sun et al., 2020). Thus, based on the hydrous pyrolysis of coal-measure source rocks under the influence of time, temperature, and pressure, we can define the processes of hydrocarbon generation, thermal characteristics of kerogen, composition and evolution of gas and liquid products, characteristics of carbon isotopes, and their response relationships with maturity. This can in turn facilitate the analysis and evaluation of the developmental situation, hydrocarbon generation potential, hydrocarbon generation material, and degree of thermal evolution in coal-measure source rocks in the Pinghu Formation, and to provide theoretical support and guidance for oil and gas exploration in the Xihu Sag.

2. Geological setting

The ECSSB was developed on the broad continental shelf of the southeast Eurasian continental segment; to its west is the Zhemin upwarping folded zone, and it is separated from the Okinawa Trough, Ryukyu island arc, and Ryukyu Trench by the Diaoyu Island upwarping folded zone in the east. The north is bordered by a ray from the Yangtze River to Jizhou Island, and the north is bordered by a ray from the Guangdong to Taiwan provinces. The basin is approximately 1,400 km long from north to south and 250–300 km wide from east to west, with a total area of approximately 26.7×10^4 km^2. Influenced by the subduction of the Philippine plate to the Eurasia plate during the Eocene to Oligocene period, the ECSSB is in a state of back-arc spreading. Simultaneously, seismic data showed apparent extension fracture activity near the NE direction, which resulted in the formation of a structural framework with nearly east-west zoning and a nearly north-south block in the plane. In addition, the ECSSB can be divided into three secondary building units: western geotectogene, central uplift belt, and eastern geotectogene from west to east. Among them, the eastern geotectogene can be classified into Diaobei Sag, Xihu Sag, and Fujiang Sag from south to north (Zhu et al., 2012; Ju et al., 2016; Chen et al., 2017; Hao et al., 2018; Zhu et al., 2019; Su et al., 2020) (Fig. 1).

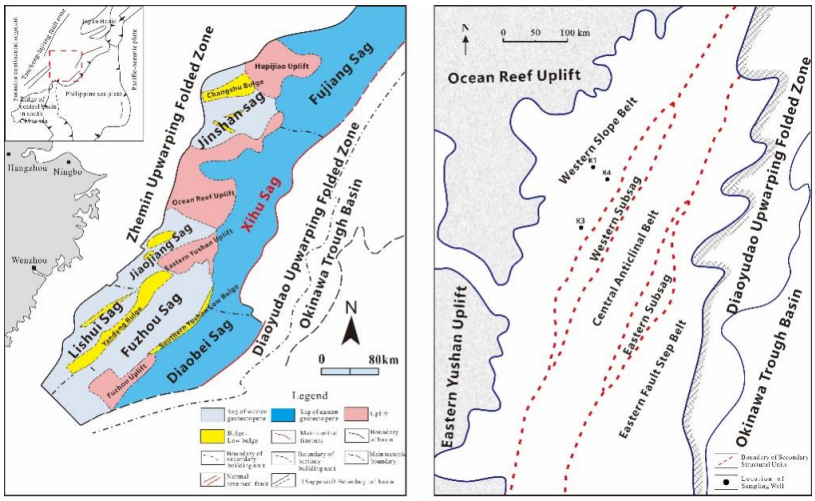

Fig. 1 Sketch map showing geographical position of tectonic units and oil and gas fields in the Xihu Sag, East China Sea Shelf basin

The Xihu Sag is located northeast of the ECSSB and belongs to a secondary sag of the western geotectogene. The Xihu Sag is approximately 400 km long from south to north and 100 km wide from east to west; it has a total area of approximately 5.18×10^4 km^2. The sedimentary thickness in the sag is approximately 9–15 km, making it the largest sedimentary sag in the ECSSB; in particular, the sedimentary characteristics indicate a great potential for oil and gas exploration and development as observed in previous studies.

The sedimentary strata drilled in the Xihu Sag were primarily the Paleogene and Neogene strata, during which there were many depositional hiatuses and regional unconformities. The Paleogene Pinghu Formation in the Xihu Sag underwent multiple tectonic movements and was deposited at the stage of tectonic thermal subsidence in the post-rift period. Consequently, the primary sedimentary facies are clastic rocks of the transitional phase. The Pinghu Formation is divided into three members from bottom to top, and each member has obvious sedimentary cycles of fine sediment in the bottom and coarse sediment on the upside. The lithology primarily comprises of yellow fine sandstone, gray siltstone, gray mudstone, and coal, with a relatively fine grain size. The distinct lithostratigraphic characteristics of the Pinghu Formation in the ECSSB were affected by tectonic and sedimentary patterns, and the overall lithology is finer from west to east (Zhang et al., 2006; Zhu et al., 2012; Lin et al., 2017; Cheng et al., 2019; Wang et al., 2021).

3. Experimental and analytical methods

3.1. Representative sample selection

Three core samples of coal-measure dark mudstone, the main type of source rock, were collected from the Upper Pinghu Formation in Wells K1, K3, and

K4 from 4,204, 3,236.7, and 4,350 m, respectively (Fig. 1). These samples were used for total organic carbon (TOC) content, Rock-Eval pyrolysis, and vitrinite reflectance (*Ro*) measurements. Only the sample from Well K4 was suitable for the formation thermal simulation experiment. Thus, the dark mudstones used in this study were collected from the upper Pinghu Formation in the K4 well (4,350–4,352 m). The basic geochemical data were: TOC: 0.68%; hydrogen index (HI): 49 mg/g TOC; *Ro*: 0.75%; and organic matter was type , which also corresponds to the typical dark mudstone in the Xihu Sag. To ensure sample uniformity, the columnar core used in the simulation experiment was a cylindrical core column formed by further pressing after crushing the samples to 40–60 mesh.

3.2. Experiments

The simulation experiment was conducted on the DK- type (third-generation) formation porosity thermocompression simulation experiment instrument from the Wuxi Research Institute of Petroleum Geology, Sinopec. The instrument had the advantages of the simulated experimental conditions approaching the actual geological conditions, retaining the original columnar and pore space, and obtaining accurate experimental data (Zheng et al., 2009; Zheng et al., 2011; Qin et al., 2014; Ma et al., 2017).

Therefore, to investigate the hydrocarbon generation potential of coal source rocks in the Pinghu Formation, we designed an experimental process based on the parameters of sedimentary and burial history, thermal evolution history, depth, and lithostatic pressure. In addition, combined with the simulated temperature, time, and pressure of the instrument, the experimental process has been detailed subsequently. 1) Experimental parameter setting: Different simulation depths were set to realize the results of simulating the different thermal evolution stages. As a result, the simulated depths were 2.8, 3.9, 4.45, 5.2, 5.9, 6.2, and 6.4 km, and the corresponding simulated temperatures were 335 °C, 360 °C, 400 °C, 455 °C, 480 °C, 525 °C, and 575 °C, respectively. The heating rate of the experiment was 1 °C/min, and after reaching the target temperature, the temperature was retained at the target temperature for 48 h. 2) Operation of the experimental instrument: After pressing the start button, the experiment commenced. 3) Acquisition and quantification of the pyrolysis products: The gaseous hydrocarbons were collected first, followed by separation and quantification of the expelled oil and residual water. Finally, the solid residues were extracted using chloroform to obtain the content of chloroform asphalt "A," which was defined as residual bitumen (Ma et al., 2017).

Stable carbon isotopes of kerogen, expelled oil, residual bitumen, and gaseous hydrocarbons at every simulated temperature point were determined using a stable isotope ratio mass spectrometer (Delta Plus V and Mat-253; Thermo Fisher Scientific, Waltham, MA, USA). The carbon isotope values were reported as -values, which are expressed as $_{\text{sample}} = (R_{\text{sample}}/R_{\text{standard}}\text{-}1) \times 1{,}000$ (‰) (where R denotes the ratio of $^{13}C/^{12}C$). The ^{13}C values were normalized to the

Pee Dee Belemnite (PDB) (Sun et al., 2015; Wu et al., 2019).

4. Results

4.1. Pyrolysis products

The correlation between the simulated temperature and measured vitrinite reflectance (*Ro*) is shown in Fig. 2. The corresponding *Ro* to these simulated temperatures of 335 °C, 360 °C, 400 °C, 455 °C, 480 °C, 525 °C, and 575 °C were 0.82%, 1.09%, 1.65%, 1.93%, 2.3%, 2.56%, and 3.24%, respectively. A clear linear positive correlation between them with a correlation coefficient (R^2) of 0.9861 was observed. Thus, this pyrolysis experiment could be seen as a continuous thermal evolution process with increasing maturity. Next, we used the value of the measured *Ro* to replace the simulated temperatures (Wu et al., 2018; Sun et al., 2019a).

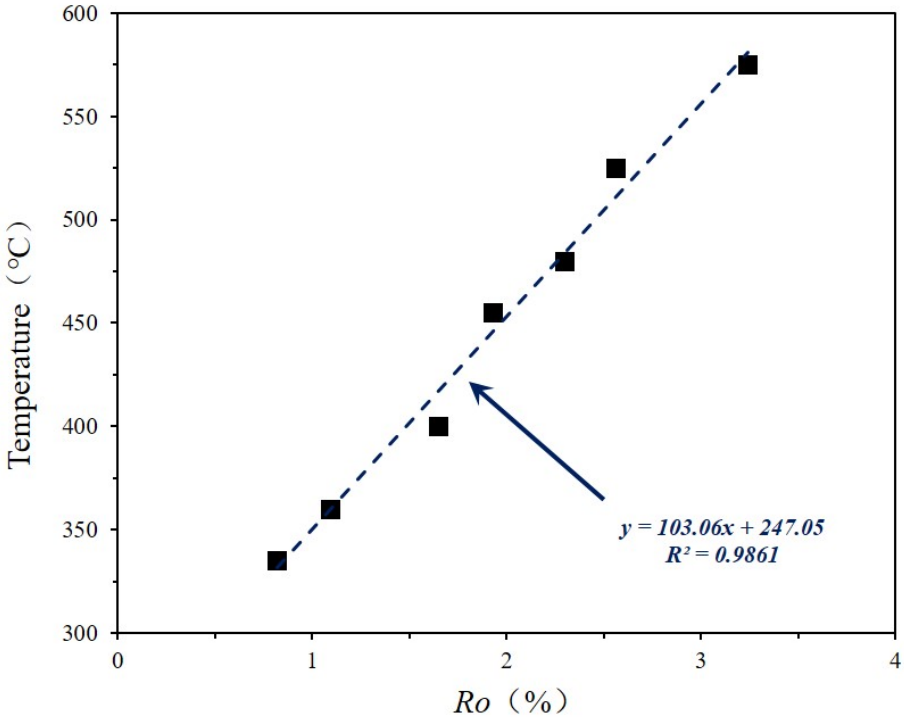

Fig. 2 The correlation between the simulated temperature and measured vitrinite reflectance (*Ro*)

The changes in gaseous hydrocarbons, expelled oil, and residual bitumen with increasing *Ro* are shown in Fig. 3. With an increase in *Ro*, the gaseous hydrocarbon yield tended to increase gradually. When *Ro* = 0.82–1.09%, the yield of gaseous hydrocarbons increased slowly with a smaller change in amplitude. When *Ro* = 1.65–2.56%, the yield of gaseous hydrocarbons increased rapidly at

a constantly increasing rate, which had a larger increase in amplitude. When Ro = 2.56–3.24%, the yield of gaseous hydrocarbons increased sharply with an increase in amplitude = 124.74%.

Overall, the yield of expelled oil first reached a specific value and remained constant at the corresponding value. The yield of expelled oil at Ro = 0.82–1.09% and corresponding simulated temperature (Ts) = 335–360 ℃ increased rapidly from 19.36 to 46.76 mg/g TOC, with an increased amplitude of 141.53%. When Ro = 0.82–1.09% (Ts = 335–360 ℃), the high amplitude of expelled oil increased slowly from 46.76 to 50.16 mg/g TOC compared with the previous thermal evolution stage. At the stage where $Ro > 1.65\%$, i.e., after the simulated temperature was higher than 400 ℃, the yield of expelled oil was 50.16, 50.07, 50.25, 50.18, and 50.22 mg/g TOC, respectively. Therefore, the yield of the expelled oil was constant.

For residual bitumen, i.e., the yield of residual oil, a continuously decreasing tendency was observed. When Ro = 0.82–1.09% (Ts = 335–360 °C, the medium maturity stage), the residual bitumen decreased from 17.78 to 17.01 mg/g TOC with increasing Ro; however, the change was not apparent. When Ro = 1.09–1.65%, the residual bitumen suddenly decreased from 17.01 to 5.7 mg/g TOC with a decreased amplitude of 66.49%. When Ro = 1.65–2.3%, a continuously declining trend slowly occurred in the yield of residual bitumen, with values of 5.70, 3.41, and 3.55 mg/g TOC. Thereafter, when $Ro > 2.56\%$, the residual bitumen decreased from 1.35 to 0.47 mg/g TOC, close to 0.

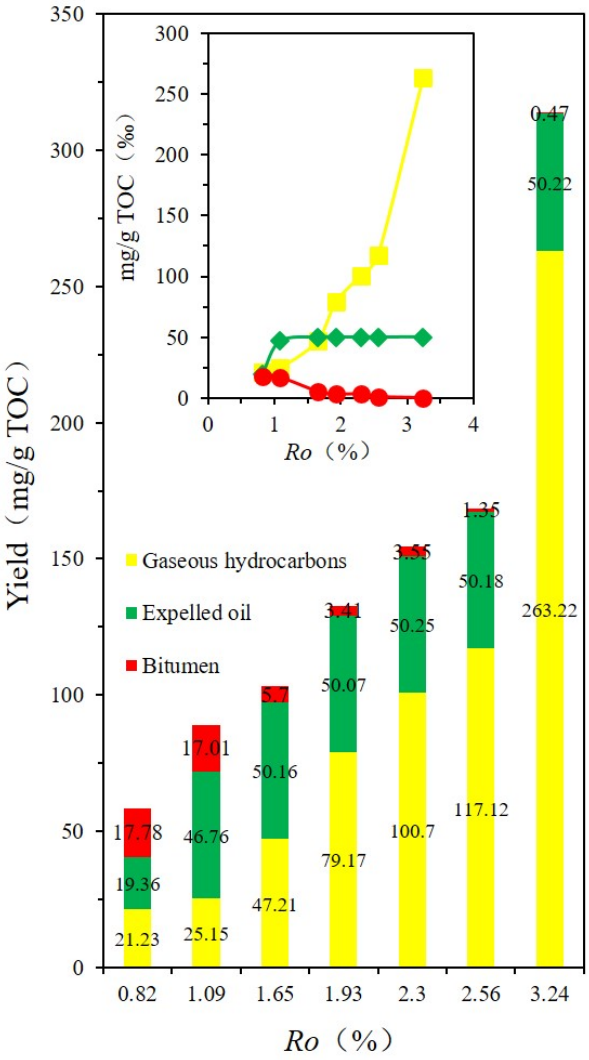

Fig. 3 The changing of gaseous hydrocarbons, expelled oil and residual bitumen with the increasing *Ro*

4.2. Stable carbon isotope composition

The ^{13}C values of kerogen, expelled oil, bitumen, and gaseous hydrocarbons are listed in Table 1 and Fig. 4.

The ^{13}C values of kerogen and bitumen in the original sample ($Ro = 0.75$) were -26‰ and -27.6‰, respectively. With an increase in *Ro*, the ^{13}C values of kerogen were -25.5‰, -25.3‰, -25.4‰, -26.1‰, -25.6‰, -25.4‰, and -25.2‰, with a mean of -25.5‰. In general, there was a tendency first to become lighter

and then heavier. When Ro = 1.93%, the carbon isotope of kerogen was the lightest, with a value of -26.1‰.

Table 1 The ^{13}C values of kerogen, expelled oil, bitumen and gaseous hydrocarbons at different simulated temperatures

Temperature	Ro	Kerogen	Expelled oil	Bitumen	CH_4	C_2H_6	C_3H_8	iC_4H_{10}	nC_4H_{10}	iC
(℃)	(%)	^{13}CPDB ‰								
Unheated	0.75	-26		-27.6						
335	0.82	-25.5	-27.5	-26.3	-39.7	-29.8	-29.3	-28.5	-28.9	-2
360	1.09	-25.3	-27.5	-26.2	-39.1	-28.3	-27.9	-28.6	-28.2	-2
400	1.65	-25.4	-27.4	-26.5	-37.1	-29.0	-29.5	-28.7	-28.7	-2
455	1.93	-26.1	-27.3	-26.1	-33.1	-27.7	-24.9	-22.9	-17.1	
480	2.30	-25.6	-26.9	-25.8	-32.2	-27.5	-20.7			
525	2.56	-25.4	-27.2	-27.0	-30.3	-24.3				
575	3.24	-25.2	-27.0	-27.5	-30.0	-19.2				

For the carbon isotope values of expelled oil, the observed values were -27.5‰, -27.5‰, -27.4‰, -27.3‰, -26.9‰, -27.2‰, and -27.0‰, with a mean of -27.3‰. Compared with the variation characteristics of carbon isotopes for kerogen, it tended to be heavier first and then lighter. Moreover, the highest value appeared at Ro = 2.3% (Ts = 480 °C), which reached -26.9‰.

The changed characteristics of carbon isotopic values on the residual oil were characterized by getting heavier first (when Ro = 0.82–1.93%, $^{13}C_{bitumen}$ = -26.3–26.1‰), and then changing sharply to the heaviest value (Ro = 2.3%, $^{13}C_{bitumen}$ = -25.8‰), after which it became lighter sharply to a value of -27.0‰ when Ro = 2.3–2.56%, and further lightened slowly to -27.5‰.

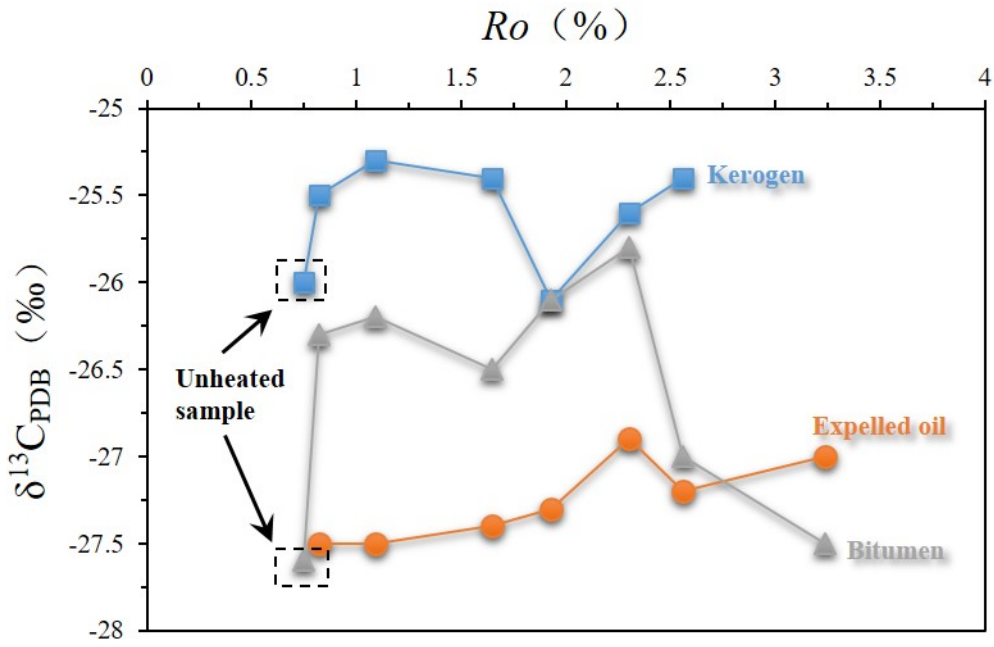

Fig. 4 The ^{13}C values of kerogen, expelled oil, bitumen and gaseous hydrocarbons at different simulated temperatures

The variation trends of carbon isotopes in gaseous hydrocarbon products with *Ro* are shown in Fig. 5, including the ^{13}C values of CH_4, C_2H_6, C_3H_8, iC_4H_{10}, nC_4H_{10}, iC_5H_{12}, and nC_5H_{12}. When *Ro* = 0.82–3.24%, $^{13}C_{CH4}$ = -39.7‰, -39.1‰, -37.1‰, -33.1‰, -32.2‰, -30.3‰, and -30.0‰ respectively, becoming heavier continuously in general. The values of $^{13}C_{C2H6}$ were -29.8‰, -28.3‰, -29.0‰, -27.7‰, -27.5‰, -24.3‰, and -19.2‰; there was a tendency for carbon isotope values to become lighter once at *Ro* = 1.09–1.65%, and all showing a tendency to be heavier at the other stages. The values of $^{13}C_{C3H8}$ ranged from -29.3‰ to -20.7‰ at *Ro* = 0.82–2.3%, except when the values changed from -27.9‰ to -29.5‰ and all the other stages became heavier. The values of $^{13}C_{iC4H10}$, were -28.5‰, -28.6‰, and -28.7‰ at *Ro* = 0.82–1.65%, which sharply increased to -22.9‰ when *Ro* = 1.65–1.93%. The variation tendency of $^{13}C_{nC4H10}$ was consistent with that of $^{13}C_{iC4H10}$, which was almost unchanged when *Ro* = 0.82–1.65%, and changed rapidly from -28.7‰ to -17.1‰ when *Ro* = 1.65–1.93%. The values of $^{13}C_{iC5H12}$ and $^{13}C_{nC5H12}$ were only measured when *Ro* = 0.82–1.65%, and both showed a trend of becoming heavier first and then lighter in a small range. In general, their carbon isotope values showed no obvious changes, which were -28.8‰, -27.2‰, and -28.6‰, and -28.8‰, -27.6‰, and -27.9‰, respectively. Overall, all the carbon isotopes of gaseous hydrocarbons tended to become heavier gradually, and among them, the carbon isotope values of methane were the lightest. Overall, the carbon sequence order was $^{13}C_{CH4} < {}^{13}C_{C2H6} < {}^{13}C_{C3H8} < {}^{13}C_{iC4H10} < {}^{13}C_{nC4H10}$ at *Ro*

1.93% (*Ts* 455 °C) and $^{13}C_{CH4} < {}^{13}C_{C2H6} < {}^{13}C_{C3H8} < (\mathbf{^{13}C_{iC4H10}} > \mathbf{^{13}C_{nC4H10}}) < {}^{13}C_{iC5H12} = {}^{13}Cn_{C5H12}$ at $Ro = 0.82\%$, which almost followed the normal carbon sequence of $^{13}C_1 < {}^{13}C_2 < {}^{13}C_3 < {}^{13}C_4 < {}^{13}C_5$ with increasing thermal evolution (Behar et al., 1992 Jarvie et al., 2007). In addition, the carbon sequence in the order of $^{13}C_{CH4} < {}^{13}C_{C2H6} < (\mathbf{^{13}C_{C3H8}} > \mathbf{^{13}C_{iC4H10}}) < {}^{13}C_{nC4H10} < (\mathbf{^{13}C_{iC5H12}} > \mathbf{^{13}C_{nC5H12}})$, at $Ro = 1.09\%$ and $^{13}C_{CH4} < {}^{13}C_{C2H6} > \mathbf{^{13}C_{C3H8}} < \mathbf{^{13}C_{iC4H10}} = {}^{13}C_{nC4H10} < \mathbf{^{13}C_{iC5H12}} < \mathbf{^{13}C_{nC5H12}}$ at $Ro = 1.65\%$, which was consistent with the evolutionary trend of $^{13}C_1 < {}^{13}C_2 > \mathbf{^{13}C_3} < {}^{13}C_4 < {}^{13}C_5$.

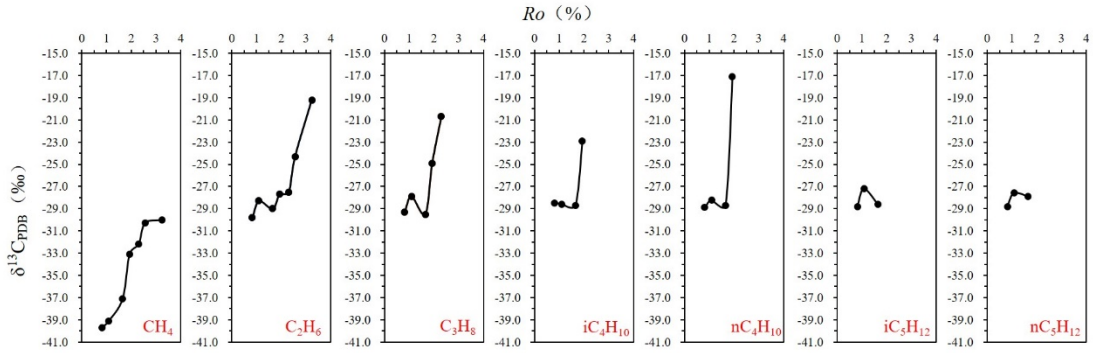

Fig. 5 The variation trend of carbon isotopes on gaseous hydrocarbon products with *Ro*

5. Discussion

5.1. Division of thermal evolution stages based on the pyrolysis products

The pyrolysis process can be divided into four stages based on the variation characteristics of the yield of expelled oil, residual bitumen, and gaseous hydrocarbons with increasing maturity (Fig. 6): 1) $Ro = 0.82$–1.09% ($Ts = 335$–360 °C), which was the lower maturity stage dominated by the generation of liquid hydrocarbons. This stage is characterized by rapid oil and lower gas generation (Tissot et al., 1974; Lewan, 1997; Hill et al., 2007; Sun et al., 2019b). The slope was used to measure the inclination of the steep curve. In mathematics, the slope of a line is the same for any point, and it is a measure of the direction and steepness of the line. The slope of a line can be calculated using principles of algebra and geometry. The slope of the curve at a point reflects how quickly the variables of the curve change at that point. When the slope (k) is positive, a greater value indicates a more rapid increase. When k is negative, a smaller value indicates a more rapid decrease (Matuszewski, 2006; Taylor et al., 2019). The slope of the curve for increased hydrocarbon yield (k_n) was equal to ($Yield_{n+1}$ - $Yield_n$) / (Ro_{n+1} - Ro_n), as shown in Table 2. At this stage, the curve of the slope for increased expelled oil ($k_{e1} = (Yield_2 - Yield_1) / (Ro_2 - Ro_1)$) reached 101.48, indicating the characteristics of rapid expelled oil generation. 2)

Ro = 1.09–1.65% (Ts = 360–400 ℃), which was the maturity stage dominated by the generation of lighter liquid hydrocarbons and wet gaseous hydrocarbons. At this stage, the yield of residual bitumen oil decreased sharply (k_b = -20.20), and the yield of expelled oil did not change significantly (k_e = 6.07, which was significantly lower than that in the first stage). The yield of hydrocarbon gases began to show an increasing trend, and the corresponding value of k also increased rapidly from 14.52 to 39.39. 3) Ro = 1.65–2.3% (Ts = 400–480 °C), the yields of gaseous hydrocarbons increased continuously, expelled oil almost did not change, and the residual oil decreased to a lower value, which could be seen as the stage of thermal cracking to wet gases. 4) Ro = 2.3–3.24% (Ts = 480–575 °C), which was the post-maturity stage. A large amount of methane was produced, and the oil and gas further cracked into methane. The increase in the amplitude of gaseous hydrocarbon was larger, and the corresponding k_g reached 172.89, providing proof of higher methane production. However, the yield of expelled oil was further reduced when the negative k_e and residual bitumen were in equilibrium with k_b near zero.

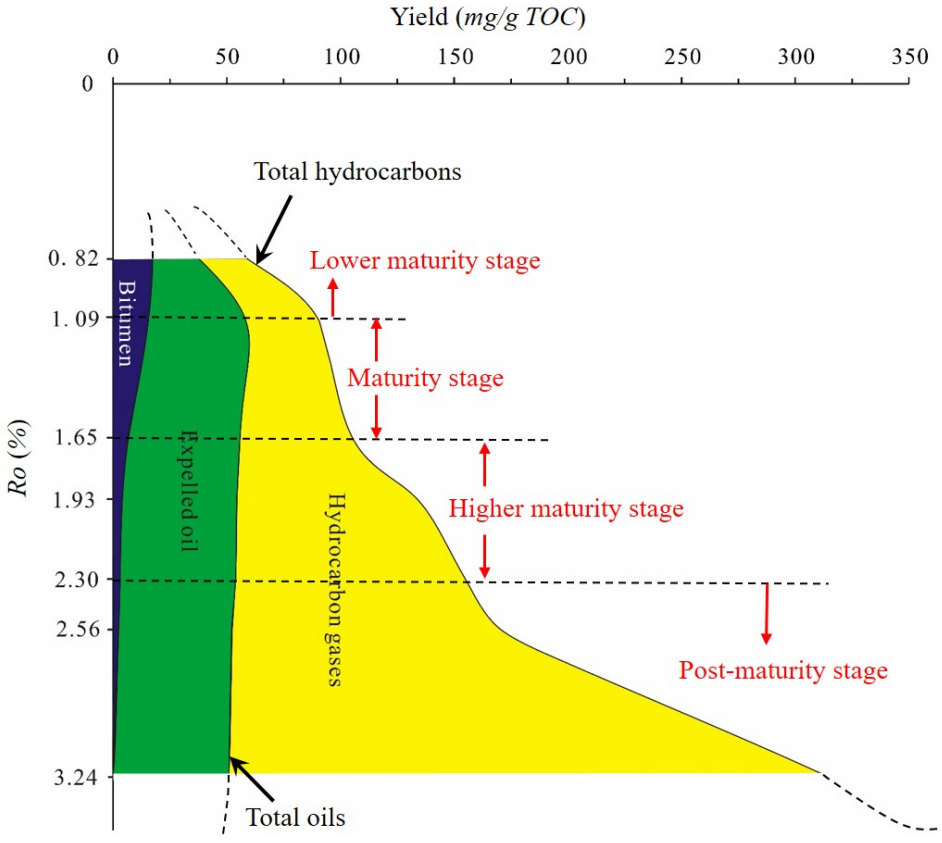

Fig. 6 The yield of expelled oil, residual bitumen and gaseous hydrocarbons

with the increasing maturity

Table 2 The slope to the curve of increased hydrocarbons yield (k_n)

The range of Ts (%)	The range of Ro (%)	stage	Linear slope	Linear slope of gaseous
335-360	0.82-1.09	Lower maturity stage	k1	14.52
360-400	1.09-1.65	Maturity stage	k2	39.39
400-480	1.65-2.30	Higher maturity stage	k3	82.29
480-575	2.30-3.24	Post-maturity stage	k4	172.89

5.2. The changing of carbon isotopes in kerogen, bitumen, expelled oil and gaseous hydrocarbons during thermal evolution stages

During thermal evolution, kerogen, expelled oil, bitumen, and gaseous products undergo a series of thermal cracking processes. Among them, the original kerogen ($kerogen_0$) and original bitumen ($bitumen_0$) exhibited a reactive nature (Tissot et al., 1978; Jarvie et al., 2007). When Ts = 335–575 °C, expelled oil, residual bitumen, and gaseous hydrocarbons of C_{2+} could not only be seen as products but also as reactants participating in the pyrolysis process. From the perspective of pyrolysis, only methane constantly remains a product during the entire thermal evolution process. Therefore, ignoring the intermediate reaction during the entire thermal evolution process, the corresponding reaction formula is as follows: *$kerogen_0$ (original) + $bitumen_0$ (original) → $kerogen_r$ (residual kerogen) + expelled oil (generated) + $bitumen_{n+r}$ (generated + residual) + C_{2+} (generated + residual) + CH_4 (generated).* In this reaction formula, the thermal evolution pathways were analyzed based on the corresponding change characteristics of carbon isotopes. Based on the principle of chemical kinetics, with changes in the coal-forming environment, organic matter type, maturity, etc., the carbon isotope composition of gases could also be changed. Simultaneously, a series of processes could produce intermediates in the cracking of kerogen, residual bitumen, or liquid hydrocarbons, and thus would result in the lighting of $^{13}C_{1\sim5}$, i.e., during thermal evolution of organic matter into hydrocarbons, the ^{12}C and ^{13}C were primarily enriched in the former and latter generated products, respectively (Kinnon et al., 2010; Papendick et al., 2011; Golding et al., 2013).

In addition, the experimental error range of ±0.5‰ for carbon isotope analysis was also considered in this analysis (Wu et al., 2018). Overall, the $^{13}C_{kerogen0}$ < $^{13}C_{kerogenr}$ and $^{13}C_{bitumen0}$ < $^{13}C_{bitumen0+r}$, and the former degree of fractionation ($^{13}C_{kerogenr}$ - $^{13}C_{kerogen0}$ = 0.1–0.8, the mean value = 0.5) was less than the latter degree of fractionation ($^{13}C_{bitumen0+r}$ - $^{13}C_{bitumen0}$ = 0.1–1.3, the mean value = 1.11), implying that kerogen and bitumen as reactants in the thermal evolution process would get heavy at their corresponding carbon isotope. In contrast, the degree of heaviness determined the strength of the reaction (Mahlstedt and Horsfield, 2012). Influenced by thermal action, the

carbon isotope of kerogen tended to become heavier in general. There was no significant difference in the weight gained between the lower maturity-maturity stage and the higher-maturity-post-maturity stage, indicating that the reaction strength of kerogen did not change much during the entire thermal evolution process. The main sources of bitumen were the residual bitumen and bitumen generated from kerogen by pyrolysis (Jarvie et al., 2007). At the lower to higher maturity stage, the carbon isotope of bitumen became heavier, suggesting that thermal evolution had a greater impact. Similarly, the original and generated bitumen were constantly parted during thermal evolution. At the post-maturity stage, the carbon isotope of the residual bitumen was fundamentally the same as that in the original bitumen, indicating that the amount of bitumen generated from kerogen was almost exhausted and reached a certain equilibrium. The remaining bitumen was that which was generated from kerogen cracking, which could also be proved by their contents, as shown in Fig. 3.

The main formation path of expelled oil was the cracking of bitumen, and the carbon isotopic composition of the expelled oil was essentially unchanged and was lighter than that in kerogen and bitumen. The yield of expelled oil was lower at the lower maturity stage and was almost in equilibrium at the higher maturity-post-maturity stage. Therefore, it can be seen that the expelled oil, as both product and reactant, was in a state of "supply and demand balance" after the maturity stage; indirectly, it showed that at the lower maturity stage, the reaction equation was kerogen $\rightarrow$ expelled oil + gaseous hydrocarbons, and dominated by the production of gaseous hydrocarbons (Tissot et al., 1978; Jarvie et al., 2007). After the maturity stage, it was dominated by the production of expelled oil. At this stage, the residual bitumen decreased continuously, indicating that the generated and increased expelled oil or gaseous hydrocarbons were further cracked into gaseous hydrocarbons to ensure the equilibrium state of the expelled oil (Castelli et al., 1990; Pepper and Corvi, 1995; Jarvie et al., 2007; Zheng et al., 2011; Qin et al., 2014; Jiang et al., 2016).

Gaseous hydrocarbons can be generated either by kerogen or by further pyrolysis of intermediate bitumen or expelled oil. Therefore, the difference in the carbon isotopes of gaseous hydrocarbons was restricted by the dynamic fractionation effect of the above two reactions. In other words, their respective isotope dynamic fractionation was closely related to the hydrocarbon formation mechanism of organic matter at different thermal evolution stages. For example, methane was the lightest carbon isotope in this study. Its generation pathway can be divided into 1) direct generation from kerogen, 2) generation from the cracking of bitumen, 3) generation from the cracking of expelled oil, and 4) generation from the secondary cracking of C_{2+} gases (Pepper and Corvi, 1995; Hill et al., 2003; Jarvie et al., 2007; Behar et al., 2008).

In general, the carbon isotope of methane showed a particularly good linear correlation with *Ro*, and the correlation equation was $^{13}C_1 = 4.632\ Ro$ - 43.493 with a correlation coefficient (R^2) of 0.9142, indicating that the carbon isotope of ^{13}C was enriched continuously with thermal evolution. The corresponding

enrichment degree of $^{13}C_1$ reached 9.7‰. The considerable carbon isotope dynamic fractionation also indicated that it was the most sensitive to maturity; therefore, it could be used for gas source correlation due to its reliability. We observed that at T_S 400℃, i.e., the low maturity-maturity stage, the enrichment degree of $^{13}C_1$ was lower at 2.6‰. However, at T_S 400 ℃, namely the high-post-maturity stage, the enrichment degree of $^{13}C_1$ increased rapidly to 9.7‰. Altogether, the results indicate the lower maturity stage was primarily controlled by kerogen and bitumen, and the main controlling factor was expelled oil and C_{2+} gases after the maturity stage. It was further proved that the formation mechanism of methane significantly differed before and after 400 °C. Moreover, according to previous studies, the secondary cracking of gaseous hydrocarbons was generally in the order of higher carbon number to lower carbon number (Behar et al., 1992; Jarvie et al., 2007; Sun et al., 2019b). When gaseous hydrocarbons with higher carbon numbers are cracked to gaseous hydrocarbons with lower carbon numbers, the carbon isotope of gaseous hydrocarbons with this carbon number deviates from the normal evolutionary track. According to the variation in the values of $^{13}C_n$- $^{13}C_{n-1}$ (n 2) with increasing *Ro* (Table 3), it can also be seen that the different corresponding difference values first decreased and then increased. The *Ro* corresponding to the lowest point was successively advanced; the larger the value of *n*, the smaller was the *Ro* at the low point of the difference value. For example, the values of $^{13}C_4$– $^{13}C_3$ demonstrated little change at $Ro = 1.09\%$ and 1.65%, those of $^{13}C_3$– $^{13}C_2$ showed a significant change between $Ro = 1.65\%$ and 1.93%, while those of $^{13}C_2$– $^{13}C_1$ showed a significant change after $Ro = 2.3\%$. In the lower evolution stage, $Ro < 1.65\%$, the cracking of gaseous hydrocarbons with higher carbon numbers was not significant. In the higher evolution stage, after $Ro > 1.65\%$, the gaseous hydrocarbons with a higher carbon number would crack into gaseous hydrocarbons with a lower carbon number successively, resulting in an increase in the difference value in the carbon isotope. Therefore, it was further explained that the formation mechanism of methane was different at different thermal evolution stages. Among them, the reactions corresponded to reaction processes 1 and 2 at the lower maturity stage, and reaction 2 was dominant. Reaction processes 1, 2, and 3 occurred at the maturity-higher maturity stage, and reaction 3 was dominant. At the post-maturity stage, reaction processes 1, 2, 3, and 4 all occurred, with reaction 4 being dominant.

Table 3 shows the variation in the values of $^{13}C_n$– $^{13}C_{n-1}$ (n 2) with increasing *Ro*

Simulated temperature(℃)	$^{13}C_2$- $^{13}C_1$	$^{13}C_3$- $^{13}C_2$	$^{13}C_{i4}$- $^{13}C_3$	$^{13}C_{n4}$- $^{13}C_3$	$^{13}C_{i5}$- $^{13}C_{i4}$	$^{13}C_{n5}$-
335	9.9	0.5	0.8	0.4	-0.3	0.1
360	10.8	0.4	-0.7	-0.3	1.4	0.6
400	8.1	-0.5	0.8	0.8	0.1	0.8
455	5.4	2.8	2.0	7.8		
480	4.7	6.8				
525	6.0					

Simulated temperature(℃)	$^{13}C_2$- $^{13}C_1$	$^{13}C_3$- $^{13}C_2$	$^{13}C_{i4}$- $^{13}C_3$	$^{13}C_{n4}$- $^{13}C_3$	$^{13}C_{i5}$- $^{13}C_{i4}$	$^{13}C_{n5}$-
575	10.8					

5.3. Ascribing meaning to the formation and exploration of oil and gas

Combined with the actual geological evolutionary conditions, they were not a definitive form of thermal evolution. Using the corresponding pyrolysis experiments, we identified the evolutionary model of different thermal evolutional stages, which helped us analyze the formation mechanisms of oil and gas in the Pinghu Formation in actual geology. The variation of methane carbon isotopes in shale gas ranged from -39.7‰ to -30.0‰ in our experiments. Cao et al. (2015) studied the composition, light hydrocarbons, and carbon isotopes of natural gases from the Xihu Sag and found that the gases were a mixture of coal type, accounting for the major proportion and oil-type gases with high maturities. In addition, they also found that the $^{13}C_1$ Xihu Sag had delta values between -47.74‰ and -28.2‰. As a result, the values of methane carbon isotopes in the process of artificial simulation fell in the range of methane carbon isotopes during the actual geological evolution process in the Xihu Depression. Thus, it can be inferred that there is great potential for coal-oil-type gases. In addition, the natural gas carbon was seen as a performance for the series of carbon isotope changes and presented the order of $^{13}C_1 < {}^{13}C_2 < {}^{13}C_1$. There was no carbon isotope reversal, which also proved the larger evolutional space. Therefore, the carbon isotope in this area can indicate the maturity of oil-gas and provide a theoretical basis and guidance for production evaluation. Combined with the analysis of geochemical characteristics of the Pinghu Formation coal-oil-type gas in actual strata, it can be considered that this area also has development potential.

6. Conclusions

This study focused on the carbon isotopic evolution of kerogen, bitumen, expelled oil, and gases during the pyrolysis of coal-measure source rocks in the Xihu Sag under semi-open conditions. In addition, we investigated the relationships between their carbon isotopes and maturity. As a result, the following conclusions were drawn:

Four thermal evolution stages occurred in the pyrolysis samples. 1) Lower maturity stage at $Ro = 0.82$–1.09% ($Ts = 335$–360 ℃), characterized by rapid oil and lower gas generation. 2) Maturity stage at $Ro = 1.09$–1.65% ($Ts = 360$–400 ℃), characterized by the generation of lighter liquid hydrocarbons and wet gaseous hydrocarbons. 3) Higher maturity stage at $Ro = 1.65$–2.3% ($Ts = 400$–480 ℃), characterized by the thermal cracking of oil to wet gases. 4) Post-maturity stage at $Ro = 2.3$–3.24% ($Ts = 480$–575 ℃), characterized by the second cracking of oil-gas to methane.

Combining the carbon isotopes of kerogen, bitumen, expelled oil, and gases

during thermal evolution, it was found that there was an obvious relationship between them. Ignoring the intermediate reaction process, the thermal evolution process can be summarized as *kerogen$_0$ (original) + bitumen$_0$ (original)* $\rightarrow$ *kerogen$_r$ (residual kerogen) + expelled oil (generated) + bitumen$_{n+r}$ (generated + residual) + C_{2+} (generated + residual) + CH_4 (generated).* The process contained both reactants and products, and only methane remained the product in each case. Therefore, the carbon isotope of methane was the lightest, and the general order was $^{13}C_{\ 1} < {}^{13}C_{\ 2\text{-}5} < {}^{13}C_{\ \text{expelled oil}} < {}^{13}C_{\ \text{bitumen}} < {}^{13}C_{\ \text{kerogen}}$. During the thermal evolution of organic matter into hydrocarbons, ^{12}C and ^{13}C were primarily enriched in the former and latter generated products, respectively. Among the products, the correlation between the methane carbon isotope and *Ro* was the most obvious, indicating that the methane carbon isotope can better characterize the corresponding maturity. Thus, based on the pyrolysis products and the carbon isotopes of oil and gases, we can clearly define the different formation mechanisms at different thermal evolution stages.

Finally, by combining the analysis of geochemical characteristics of the Pinghu Formation coal-oil-type gas in actual strata with these pyrolysis experiments, it was concluded that this area also had substantial development potential.

Acknowledgments:

We thank CNOOC Shanghai Branch for providing valuable opportunity for sampling and geological data. We thank Sinopec Wuxi Institute of Petroleum Geology for providing valuable opportunity for experimental conditions and technical support. In addition, this study was supported by National Science and Technology Major Project of China (No.2016ZX05027001-005) National Natural Science Foundation of China (No. 40172051).

References

1. Behar, F., Kressmann, S., Rudkiewicz, J.L., Vandenbroucke, M., 1992. Experimental simulation in a confined system and kinetics modelling of kerogen and oil cracking. Org. Geochem. 19(1-3), 173-189.
2. Behar, F., Lorant, F., Lewan, M., 2008. Role of NSO compounds during primary cracking of a Type II kerogen and a Type III lignite. Org. Geochem. 39, 1-22.
3. Braun, R.L., Bumham, A.K., 1990. Mathematical model of oil generation, degradation and expulsion. Energy Fuel 121, 4(1), 132-146.
4. Castelli, A., Chiaramonte, M.A., Beltrame, P.L., Carniti, P., Del Bianco, A., Stroppa, F., 1990. Thermal degradation of kerogen by hydrous pyrolysis. Org. Geochem. 16(1-3), 75-82.
5. Chen, Y.Z., Xu, Z.X., Xu, G.S., Xu, F.H., Liu, J.S., 2017. Coupling relationship between abnormal overpressure and hydrocarbon accumulation in a central overturned structural belt, Xihu Sag, East China Sea Basin (In Chinese with English abstract). Oil Gas Geol. 38 (3), 570–581.

6. Cheng, X , Hou, D., Zhao, Z., Jiang, Y., Zhou, X., Diao, H., 2020. Higher landplant -derived biomarkers in light oils and condensates from the coal-bearing eocene pinghu formation, xihu sag, east china sea shelf basin. J. Petrol. Geol. 43(4), 437-452.

7. Cheng, X., Hou, D., Zhao, Z., Chen, X., Diao, H., 2019.Sources of Natural Gases in the Xihu Sag, East China Sea Basin: Insights from Stable Carbon Isotopes and Confined System Pyrolysis. Energy Fuel 33, 2166-2175.

8. Connan, J., 1974. Time-temperature relation in oil genesis. AAPG Bull. 58(12), 2516-2521.

9. Cramer, B., Krooss, B.M., Littke, R., 1998. Modelling isotope fractionation during primary cracking of natural gas: a reaction kinetic approach. Chem. Geol. 149, 235-250.

10. Dai, J., Zou, C., Li, J., Ni, Y., Hu, G., Zhang, X., Liu, Q., Ynag, C., Hu, A., 2009. Carbon isotopes of Middle-Lower Jurassic coal-derived alkane gases from the major basins of northwestern China. Int. J. Coal Geol. 80, 124-134.

11. Fu, D., Xu, G., Ma, L. Yang, F., Ma, Y., 2020. Gas generation from coal: taking Jurassic coal in the Minhe Basin as an example. Int J Coal Sci Technol 7, 611-622.

12. Golding, S.D., Boreham, C.J., Esterle, J.S., 2013. Stable isotope geochemistry of coal bed and shale gas and related production waters: a review. Int. J. Coal Geol. 120, 24-40.

13. Hao, L. , Wang, Q. , Tao, H. , Li, X. , Ma, D. , Ji, H., 2018. Geochemistry of oligocene huagang formation clastic rocks, xihu sag, the east china sea shelf basin: provenance, source weathering, and tectonic setting. Geol. J. 53, 397-411.

14. Hill, R.J., Jarvie, D.M., Zumberge, J., Henry, M., Pollastro, R.M., 2007. Oil and gas geochemistry and petroleum systems of the Fort Worth Basin. AAPG Bull. 91(4), 445-473.

15. Hill, R.J., Tang, Y.C., Kaplan, I.R., 2003. Insights into oil cracking based on laboratory experiments. Org. Geochem. 34, 1651-1672.

16. Jarvie, D.M., Hill, R.J., Ruble, T.E., Pollastro, R.M., 2007. Unconventional shale-gas systems: The Mississippian Barnett Shale of north-central Texas as one model for thermogenic shale-gas assessment. AAPG bull. 91(4), 475-499.

17. Jiang, S., Li, S., Chen, X., Zhang, H., Wang, G., 2016. Simulation of oil-gas migration and accumulation in the East China Sea continental Shelf basin: a case study from the Xihu depression. Geol. J. 51, 229-243.

18. Ju, C.X., Dong, C.M., Zhang, X.G., Dong, Y.X., 2016. Study on the pore structure of low permeability reservoir of the Huagang Formation in Xihu

Depression area (In Chinese with English abstract). Mar. Geol. Front. 32 (9), 32-40.

19. Kinnon, E.C.P., Golding, S.D., Boreham, C.J., Baublys, K.A., Esterle, J.S., 2010. Stable isotope and water quality analysis of coalbed methane production waters and gases from the Bowen Basin, Australia. Int. J. Coal Geol. 82, 219-231.

20. Krouse, H.R., Viau, C.A., Eliuk, L.S., Ueda, A., Halas, S., 1988. Chemical and isotopic evidence of thermochemical sulfate reduction by light-hydrocarbon gases in deep carbonate reservoirs. Nat. 333(6172), 415-419.

21. Leif, R.N., Simoneit, B.R.T., 2000. The role of alkenes produced during hydrous pyrolysis of a shale. Org. Geochem. 31(11), 1189-1208.

22. Lewan, M.D., 1997. Experiments on the role of water in petroleum formation. Geochim. Cosmochim. Ac. 61(17), 3691-3723.

23. Lewan, M.D., Winters, J.C., McDonald, J.H., 1979. Generation of oil-like pyrolyzates from organic-rich shales. Sci. 203(4383), 897-899.

24. Lin, C.Y., Sun, X.L., Ma, C.F., Zhang, X.G., Zhao, Z.X., 2017. Physical property evolution of Huagang formation in central inversion tectonic belt in Xihu depression (In Chinese with English abstract). J. China Inst. Min. Technol. 46 (4), 700-709.

25. Ma, Z., Zheng, L., Xu, X., Bao, F., Yu, X., 2017. Thermal simulation experiment of organic matter-rich shale and implication for organic pore formation and evolution. Petrol. Res. 2(4), 347-354.

26. Mahlstedt, N., Horsfield, B., 2012. Metagenetic methane generation in gas shales I.Screening protocols using immature samples. Mar. Petrol. Geol. 31, 27-42.

27. Matuszewski, B.K., 2006. Standard line slopes as a measure of a relative matrix effect in quantitative HPLC-MS bioanalysis. J. Chromat. B. 830 (2), 293-300.

28. Papendick, S.L., Downs, K.R., Vo, K.D., Hamilton, S.K., Dawson, G.K.W., Golding, S.D., Gilcrease, P.C., 2011. Biogenic methane potential for Surat basin, Queensland coal seams. Int. J. Coal Geol. 88, 123-134.

29. Pepper, A.S., Corvi, P.J., 1995. Simple kinetic models of petroleum formation. Part I: oil and gas generation from kerogen. Mar. Petrol. Geol., 12(3), 291-319.

30. Pepper, A.S., Dodd, T.A., 1995. Simple kinetic models of petroleum formation. Part II: oil-gas cracking. Mar. Petrol. Geol. 12(3): 321-340.

31. Prinzhofer, A.A., Huc, A.Y., 1995. Genetic and post-genetic molecular and isotopic fractionations in natural gases. Chem. Geol. 126, 281-290.

32. Qin, J., Shen, B., Tao, G., Teng, E., Yang, Y., Zheng, L., Fu, X., 2014. Hydrocarbon- forming organisms and dynamic evaluation of hydrocarbon generation capacity in excellent source rocks. Petro. Geol. Exper. 36(4), 465-472.

33. Schimmelmann, A., Boudou, J.P., Lewan, M.D., Wintsch, R.P., 2001. Experimental controls on D/H and $^{13}C/^{12}C$ ratios of kerogen bitumen and oil during hydrous pyrolysis. Org. Geochem. 32(8), 1009-1018.

34. Su, A., Chen, H., Lei, M., Li, Q., Wang, C., 2019. Paleo-pressure evolution and its origin in the Pinghu slope belt of the Xihu Depression, East China Sea Basin. Mar. Petrol. Geol. 107, 198-213

35. Su, A., Chen, H., Zhao, J., Zhang, T., Feng, Y., Wang, C., 2020. Natural gas washing induces condensate formation from coal measures in the Pinghu Slope Belt of the Xihu Depression, East China Sea Basin: Insights from fluid inclusion, geochemistry, and rock gold-tube pyrolysis. Mar. Petrol. Geol. 118, 104450.

36. Su, A., Chen, H.H., Chen, X., He, C., Liu, H.P., Li, Q., Wang, C.W., 2018. The characteristics of low permeability reservoirs, gas origin, generation and charge in the central and western Xihu depression, East China Sea Basin. J. Nat. Sci. Eng. 53, 94-109.

37. Sun, L., Fu, D., Chai, S., Yang, W., Zhou, K., Li, W., 2020. Fractal characteristics and significances of the nanopores in oil shales during hydrous pyrolysis. J. Petrol. Explor. Prod. Tech. 10(2), 557-567.

38. Sun, L., Tuo, J., Zhang, M., Wu, C., Chai, S., 2019a. Impact of Water Pressure on the Organic Matter Evolution from Hydrous Pyrolysis. Energy Fuel. 33, 6283-6293.

39. Sun, L., Tuo, J., Zhang, M., Wu, C., Chai, S., 2019b. Pore structures and fractal characteristics of nano-pores in shale of Lucaogou formation from Junggar Basin during water pressure-controlled artificial pyrolysis. J. Anal. Appl. Pyrol. 140, 404-412.

40. Sun, L., Tuo, J., Zhang, M., Wu, C., Wang, Z., Zheng, Y., 2015. Formation and development of the pore structure in Chang 7 Member oil-shale from Ordos Basin during organic matter evolution induced by hydrous pyrolysis Fuel 158, 549-557.

41. Takahashi, K.U., Suzuki, N., Saito, H., 2014. Compositional and isotopic changes in expelled and residual gases during anhydrous closed-system pyrolysis of hydrogen-rich Eocene subbituminous coal. Int. J. Coal Geol. 127, 14-23.

42. Taylor, R., Duss, M., 2019. A paper about the slope of the equilibrium line. Chem. Eng. Res. Des.148, 429-439.

43. Tissot, B.P., Durand, B. Espitalie, J. Combaz, A., 1974. Influence of mature and diagenesis of organic matter in the formation of petroleum. AAPG Bull. 58(3), 499-506.

44. Wang, W., Lin, C., Zhang, X., Dong, C., Ren, L., Lin, J., 2021. Provenance, clastic composition and their impact on diagenesis: A case study of the Oligocene sandstone in the Xihu sag, East China Sea Basin. Mar. Petrol. Geol 126, 104890,

45. Waples, D.W., 2000. The kinetics of in-reservoir oil destruction and gas formation: constraints from experimental and empirical data, and from thermodynamics. Org. Geochem. 31(6), 553-575.

46. Wu, Y., Zhang, Z., Sun, L., Li, Y., Zhang, M., Ji, L., 2019. Stable isotope reversal and evolution of gas during the hydrous pyrolysis of continental kerogen in source rocks under supercritical conditions. Int. J. Coal Geol. 205, 105-114.

47. Xie, G., Shen, Y., Liu, S., Hao, W., 2018. Trace and rare earth element (REE) characteristics of mudstones from Eocene Pinghu Formation and Oligocene Huagang Formation in Xihu Sag, East China Sea Basin: Implications for provenance, depositional conditions and paleoclimate. Mar. Petrol. Geol. 92, 20-36.

48. Xu, H., George, S.C., Hou, D., Cao, B., Chen, X., 2020. Petroleum sources in the Xihu Depression, East China Sea: Evidence from stable carbon isotopic compositions of individual n-alkanes and isoprenoids. J. Petrol. Sci. Eng. 190, 107073.

49. Zhang, Z.M., Zhou, J., Wu, X.W., 2006. Oil and gas migration periods and accumulation process in central anticlinal zone in the Xihu sag, the East China Sea Basin (In Chinese with English abstract). Petrol. Geol. Exp. 28 (1), 30-37.

50. Zhao, W., Zhang, S., Wang, F., Cramer, B., Chen, J., Sun, Y., Zhang, B., Zhao, M., 2005. Gas systems in the Kuche Depression of the Tarim Basin: Source rock distributions, generation kinetics and gas accumulation history. Org. Geochem. 36(12), 1583-1601.

51. Zheng, L., Ma, Z., Wang, Q., Li, Z., 2011. Quantitative evaluation of hydrocarbon yielding potential of source rock: application of pyrolysis in finite space. Petrol. Geol. Exper. 33(5), 452-459

52. Zheng, L.J., Qin, J.Z., He, S., Li, G.Y., Li, Z.M., 2009. Preliminary study of formation porosity thermocompression simulation experiment of hydrocarbon generation and expulsion. Pet. Geol.Exp. 31 (3), 296-302. (in Chinese).

53. Zhu, W., Zhong, K., Fu, X., Chen, C., Zhang, M., Gao,S., 2019. The formation and evolution of the East China Sea Shelf Basin: A new view. Earth Sci. Rev. 190, 89-111.

54. Zhu, X., Chen, J., Li, W., Pei, L., Liu, K., Chen, X., Zhang, T., 2020. Hydrocarbon generation potential of Paleogene coals and organic rich mudstones in Xihu sag, East China Sea Shelf basin, offshore eastern China, J. Petrol. Sci. Eng. 184, 106450.

55. Zhu, Y.M., Li, Y., Zhou, J., Gu, S.X., 2012. Geochemical characteristics of tertiary coalbearing source rocks in Xihu depression, East China Sea Basin. Mar. Pet. Geol. 35,154-165.